Supplementary information

Size segregated particle number and mass emissions in urban Beijing

Jing Cai[1,2], Biwu Chu[1,2,3,4], Lei Yao[2], Chao Yan[1,2], Liine M. Heikkinen[1,2], Feixue Zheng[1], Chang Li[1], Xiaolong Fan[1], Shaojun Zhang[5], Daoyuan Yang[5], Yonghong Wang[2], Tom V. Kokkonen[1,2], Tommy Chan[1,2], Ying Zhou[1], Lubna Dada[1,2], Yongchun Liu[1], Hong He[3,4], Pauli Paasonen[1,2], Joni T. Kujansuu[1,2], Tuukka Petäjä[1,2], Claudia Mohr[6], Juha Kangasluoma[1,2], Federico Bianchi[1,2], Yele Sun[7], Philip L. Croteau[8], Douglas R. Worsnop[2,8], Veli-Matti Kerminen[1,2], Wei Du[1,2]*, Markku Kulmala[1,2]*, Kaspar R. Daellenbach[1,2]*

[1] Aerosol and Haze Laboratory, Beijing Advanced Innovation Center for Soft Matter Science and Engineering, Beijing University of Chemical Technology, Beijing, 100029, China

[2] Institute for Atmospheric and Earth System Research, Faculty of Science, University of Helsinki, Helsinki, 00014, Finland

[3] Center for Excellence in Regional Atmospheric Environment, Institute of Urban Environment, Chinese Academy of Sciences, Xiamen, 361021, China

[4] State Key Joint Laboratory of Environment Simulation and Pollution Control, Research Center for Eco-Environmental Sciences, Chinese Academy of Sciences, Beijing, 100085, China

[5] School of Environment, Tsinghua University, Beijing, 100084, China

[6] Department of Environmental Science, Stockholm University, Stockholm, 11418, Sweden

[7] State Key Laboratory of Atmospheric Boundary Layer Physics and Atmospheric Chemistry, Institute of Atmospheric Physics, Chinese Academy of Sciences, Beijing, 100029, China

[8] Aerodyne Research, Inc., Billerica, MA, 01821, USA

Correspondence to: Wei Du (wei.du@helsinki.fi), Markku Kulmala (markku.kulmala@helsinki.fi) and Kaspar R. Daellenbach (kaspar.daellenbach@gmail.com)

1. RIEs and CO_2^+/ NO_3 artifact correction of ACSM

The relative ionization efficiencies (RIEs) for sulfate, nitrate, ammonium, chloride and organics were 0.86, 1.05, 4.0, 1.5 and 1.4, respectively. RIEs of ammonium, sulfate and chloride were obtained by pure standard of NH_4NO_3 (99%, Tianjin-Fuchen Corp. China), $(NH_4)_2SO_4$ (99 %, Sigma-Aldrich Corp. U.S.) and NH_4Cl (99.5%, Sigma-Aldrich Corp. U.S.). Ionization efficiency (IE) in this study was obtained from ammonium nitrate calibration, which was 167.6 ions/pg under air beam of 3.1×10^5 ions/s.

Recently, it was discovered that NO_3 induces a positive bias on organic CO_2^+ concentrations in the AMS/ACSM systems by Pieber et al. (2016), which can be described as a function of ambient NO_3 ($\mu g/m^3$) in combination with the CO_2^+/NO_3 ratio from pure NH_4NO_3 measurements $(CO_2^+/NO_3)_{AN}$:

For pure NH_4NO_3 aerosol from calibrations, we determined the magnitude of the CO_2^+/NO_3 artifact(Pieber et al., 2016) and parametrized it as a function of the fragmentation pattern of NO_3 (NO^+/NO_2^+) to account for changes in the vaporizer in the ACSM:

$$(CO_2^+/NO_3)_{NH4NO3} = 0.025 \pm 0.002 \times (NO^+/NO_2^+)_{NH4NO3}$$

Then we determined the CO_2 concentration from OA using a two week moving average (NO^+/NO_2^+) from ambient observations:

$$(CO_2^+)_{OA,meas} = (CO_2^+)_{meas} - (CO_2^+/NO_3)_{NH4NO3} \times (NO_3)_{meas}$$

Further, we propagated the uncertainty of the subtraction when computing the PMF input matrices.

$$\sigma_{(CO2+)_{OA,meas}} = \sqrt{\sigma_{((CO2+)_{OA,meas})counting}{}^2 + \sigma_{((CO2+NO3)_{AN,meas}\times(NO3)_{meas})}{}^2}$$

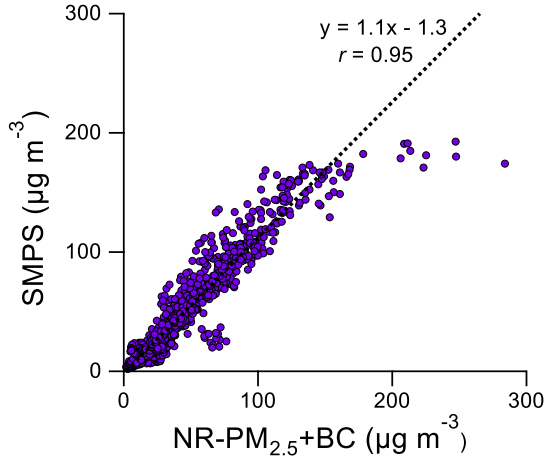

Fig. S1 Comparison of calculated PM_{SMPS} with measured NR-$PM_{2.5}$ plus BC in all sampling days

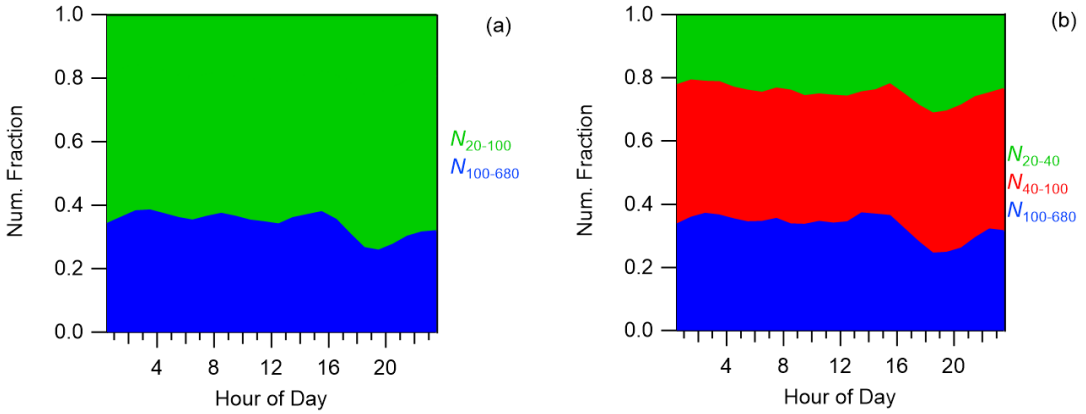

Fig. S2 Average diurnal evolution of number fractions of (a) $N_{20\text{-}100}$ (20–100 nm) and $N_{20\text{-}100}$ (100–680 nm), (b) number concentrations in $N_{20\text{-}40}$ (20–40 nm), $N_{40\text{-}100}$ (40–100 nm) and $N_{100\text{-}680}$ (100–680 nm) during non-NPF days

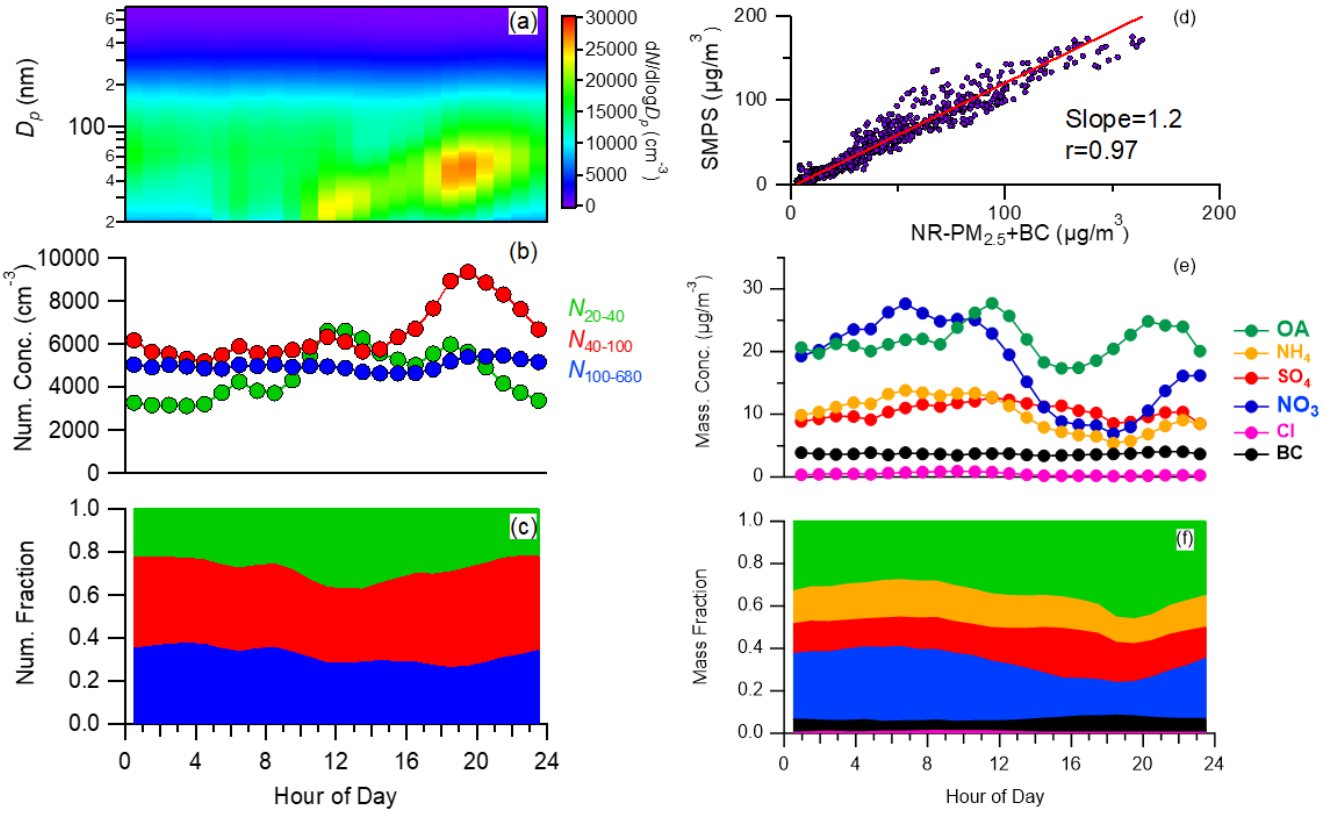

Fig. S3 Average diurnal evolution of particle number size distribution during all days (NPF days are also concluded). (a) Particle size distribution, (b) number concentrations in $N_{20\text{-}40}$ (20–40 nm), $N_{40\text{-}100}$ (40–100 nm) and $N_{100\text{-}680}$ (100–680 nm), (c) number fractions, (d) the comparison between SMPS and NR-$PM_{2.5}$+BC, (e) different component concentrations (f) and diurnal variations of the mass fractions of different components

And to compare our sampling period with long-term measurement, we also present the NR-$PM_{2.5}$ and BC measured from Feb 2018 to Jun 2019, which is shown in Figure S4.

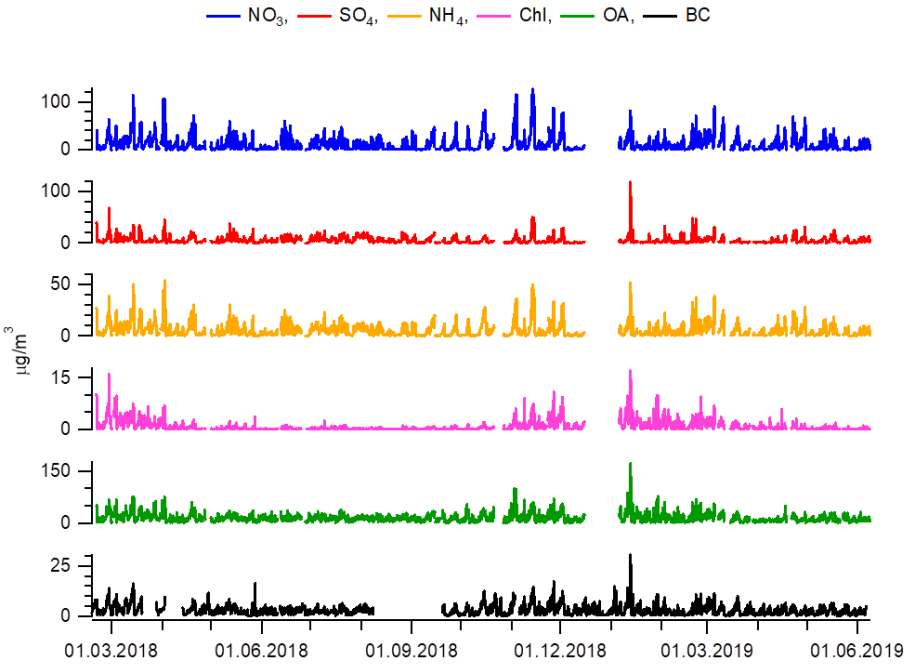

Fig. S4 Long-term (Feb 2018 to Jun 2019) measurement of NR-$PM_{2.5}$ from ACSM and BC from aethalometer

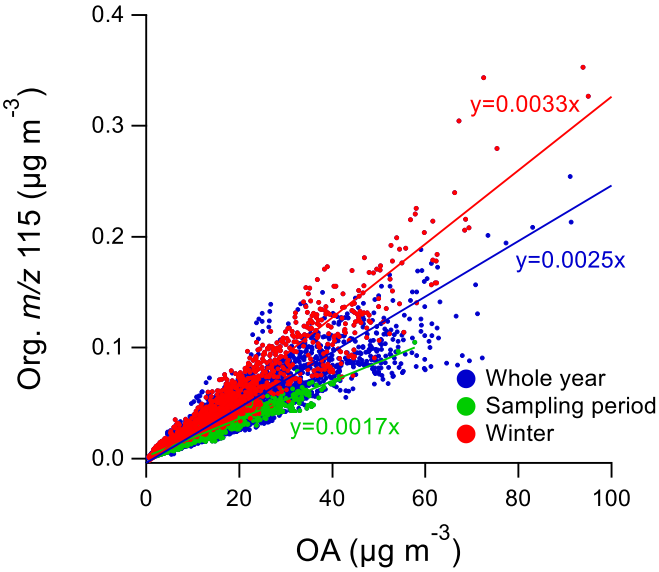

Figure S5. The ratio of *m/z* 115 to total OA in our sampling period (April 6 to July 2, 2018), winter period (Dec 2018 to Feb 2019) and the whole year measurement (Feb 2018 to Jun 2019).

2. PMF analysis and validations

2.1 Size-PMF validations

Table S1. NPF days during the sampling period (April 6, 2018 to July 2, 2018)

Month	Day of the Month
April, 2018	10, 11, 12, 15, 16, 17, 24, 25, 27, 30
May, 2018	1, 2, 3, 5, 6, 7, 8, 9, 18, 22, 23, 24, 27, 28, 29, 30
June, 2018	1, 2, 4, 13, 17, 19, 20, 21, 23, 24, 25, 27, 28

PMF (2, ver. 4.2 (Ulbrich et al., 2009)) is applied to the size-resolved particle number concentrations. Q/Q_{exp} decreases when the number of factors increases (Fig. S6). Five factors can already explain the whole dataset well. After adding more factors, large size components are separated to several small sub-groups, which cannot explained by environmental process. Therefore, we employ five factors in this analysis.

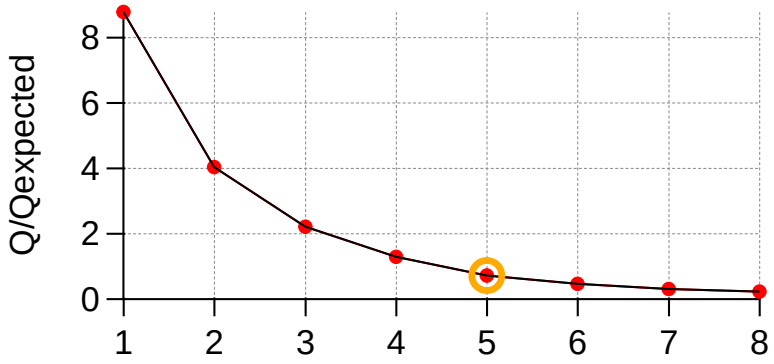

Fig. S6 Q/Q_{exp} as a function of the number of factors in Size-PMF analysis

Fpeak tests are conducted with the range of -1 to 1 (increments 0.2). Compared to base case runs, fpeak rotations only change the separation and profiles of the factors explaining particles with large sizes and hypothetical regional origin (Factor 4 and 5, Fig S7) with negative fpeak values. The most significant variations occur in Factors 5 with negative fpeak values, which has very low concentrations (Fig. S7 (f)). Positive fpeak values can help to pull the profile of large size components into several modes, which is more similar to the particles coming from regional sources. In addition, according to the residuals, the explanations of large particles are also better with positive Fpeak runs. Thus, we take the fpeak of 1.0 as the results of Size-PMF.

Both profiles and contributions from primary sources (Factor 1, 2 and 3) are stable among all the fpeak runs (Fig. S7 and S6), which is also validated by bootstrap analysis (Fig. S8). Those analyses show the stability of the Size-PMF results.

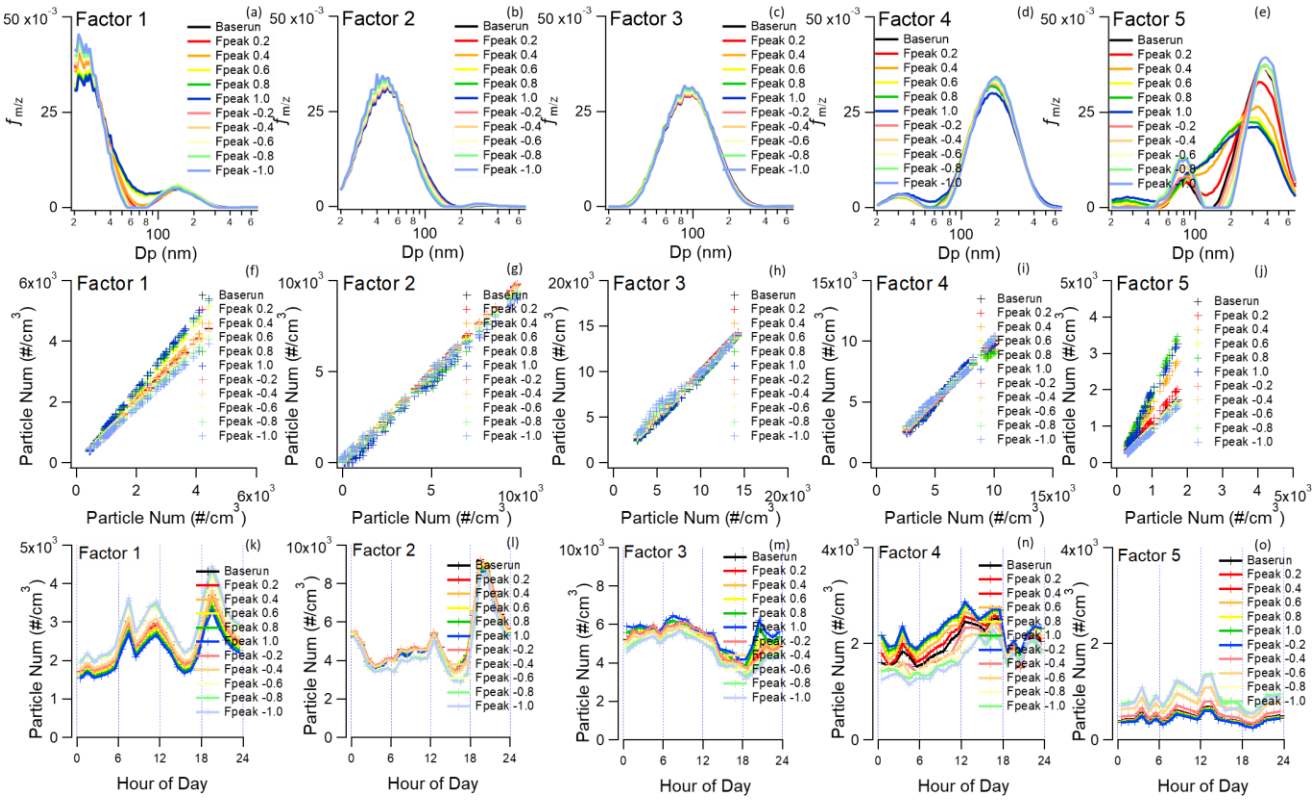

Fig. S7 Profiles of different factors with different Fpeak values resolved in size-PMF (sub-fig (a) to (e)) and time series of different factors with different Fpeak values resolved in size-PMF (sub-fig (f) to (j))

Further, we assess the stability of the Size-PMF results through bootstrapping the PMF input (200 iterations). Primary sources (Factor 1, 2 and 3) are stable both in terms of their factor profiles as well as their contributions, while regional sources show larger variations in the large size range, supporting the state that the primary sources are well resolved. The residual to uncertainty ratio (scaled residual) also suggests larger uncertainties in explaining the variability of the largest particles. The time series of scale residual exhibits no clear trend (Fig. S9 (b)).

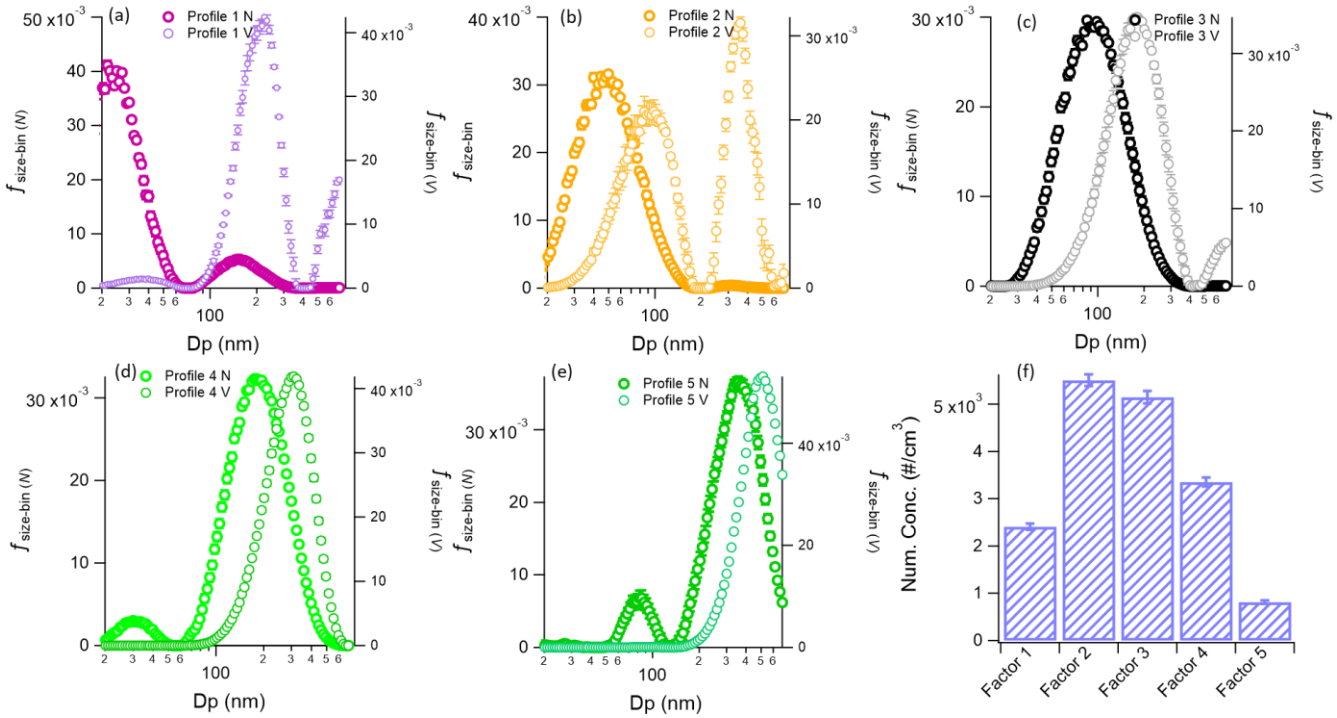

Fig. S8 Number profile and volume profiles of different factors in bootstrap runs (sub-fig (a) to (e)). Round dots and error bars represent the average value and one standard variation of all solutions, respectively. Average number concentration of different factors with one standard variation of all runs is displayed in sub-fig (f)

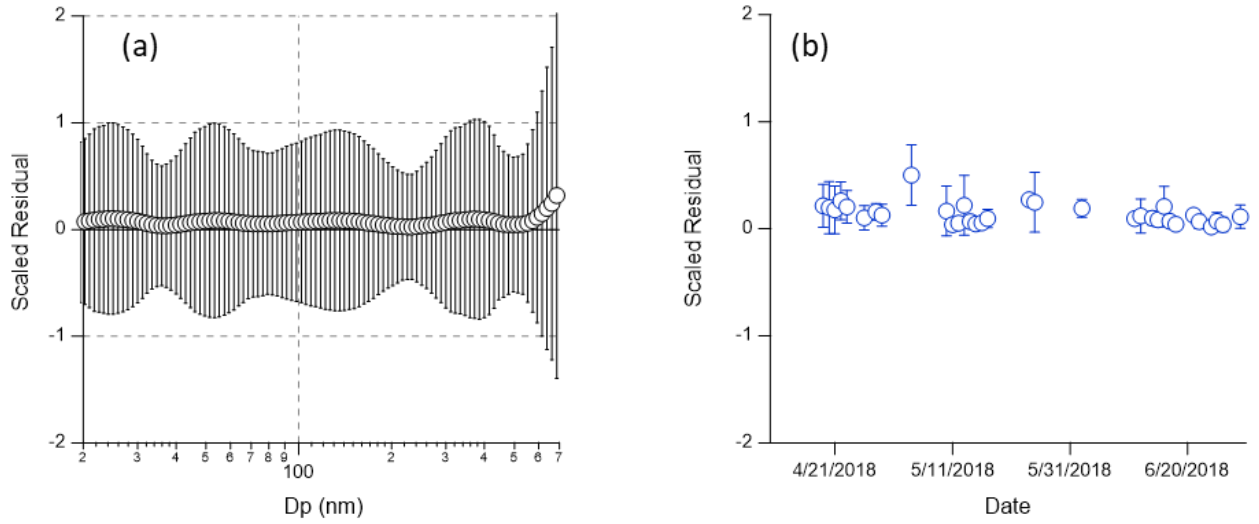

Fig. S9 Scaled residual as a function of Dp (a) and date (b) in Size-PMF analysis, round dots represent mean Scaled residual and error bars represent the standard deviation. Rescale residual is defined as the ratio of residual to uncertainty

2.2 OA-PMF validations

Prior to OA-PMF analysis, we tested constraining cooking, gasoline and diesel profiles in order to test whether vehicular emissions can be separated according to the fuel type. We performed 300 PMF runs times using a random a-value in the range of 0 to 0.1 independently for HOA and COA (increment of 0.05). A relatively small a-value is applied due to the high similarity of the profiles from gasoline and diesel exhausts. The results show clear indications that gasoline and cooking emissions are mixed (similar diurnals, Fig. S10). Based on this test, it seems not possible to separate vehicular emissions based on the fuel type used in our dataset.

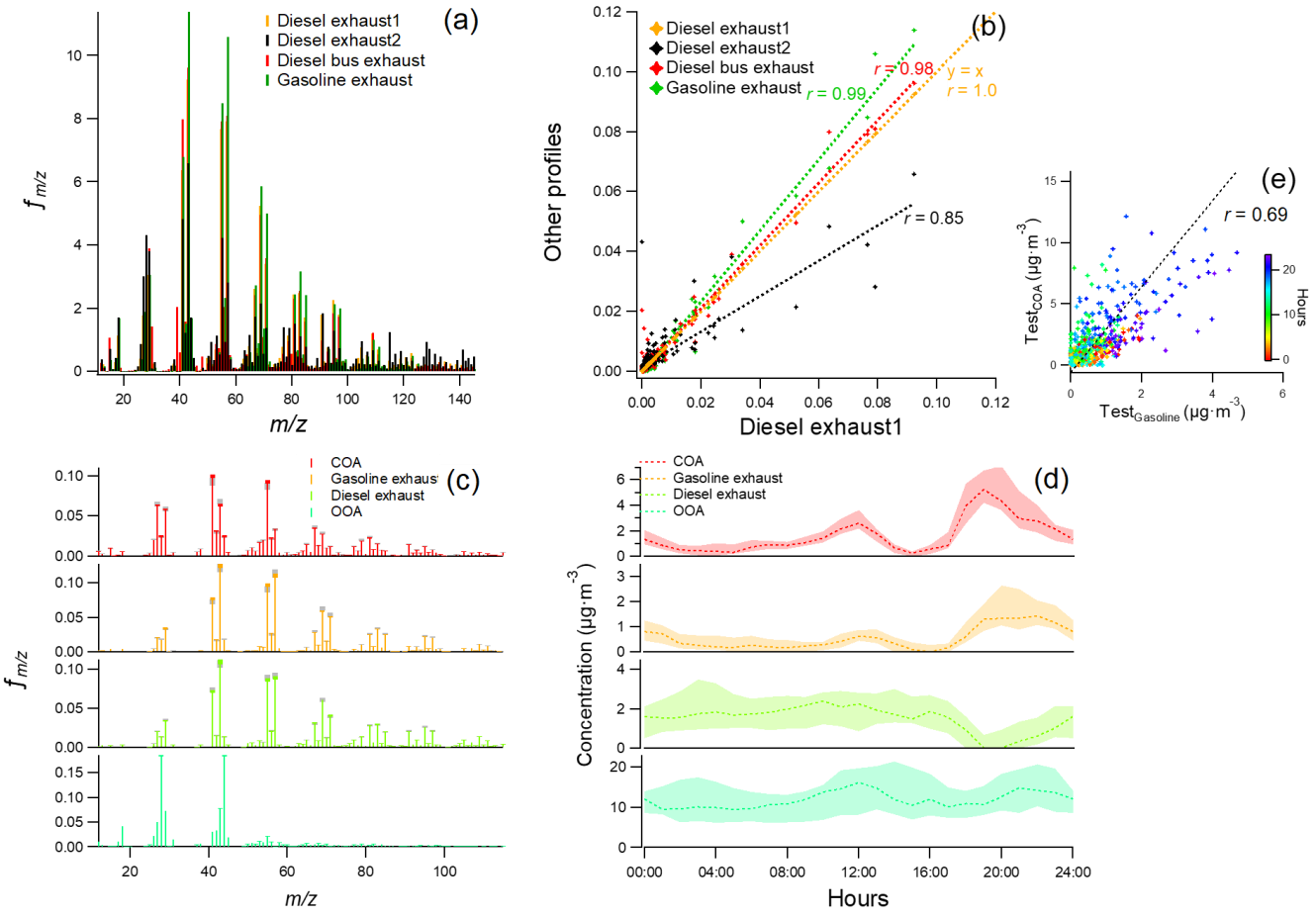

Fig. S10 (a) comparison of source profiles for vehicular exhaust tests, data source: Diesel exhaust 1 (Mohr et al., 2009), Diesel 2 (Sage et al., 2008), Diesel bus exhaust (Canagaratna et al., 2004), gasoline exhaust (Mohr et al., 2009), (b) correlations of source profiles of vehicular exhausts. PMF results (constrained gasoline, diesel, and cooking reference spectra from Mohr et al. (2009), (Canagaratna et al., 2004) and Crippa et al. (2013b), respectively with a-value between 0 and 0.1), c) PMF factor profiles, (d) diurnal variations of PMF factor time series, (e) resolved COA concentrations as a function of gasoline factor concentrations

In OA-PMF analysis, organic mass spectra are imported and analyzed by the multi-linear engine (ME-2) algorithm (ME-2) implemented in the toolkit SoFi, Source Finder. Unconstrained runs exhibit that a mixed POA (primary OA) component and a SOA (secondary OA) component. According to numerous previous researches in Beijing, during our sampling period, BBOA (biomass burning OA) and CCOA (coal combustion OA) are usually the lowest throughout the year(Sun et al.,

2018;Hu et al., 2017). To separate the primary sources, the mass spectral fingerprint of HOA and COA from Crippa (Crippa et al., 2013a;Crippa et al., 2013b) are applied to constrain the PMF runs. Since adding factors cannot further decrease Q/Q_{exp} ratio, four-factor result is chosen (Fig. S11). In the next step, we perform sensitivity tests by performing 2500 PMF runs times using a random a-value in the range of 0 to 1 independently for HOA and COA(increment of 0.1).

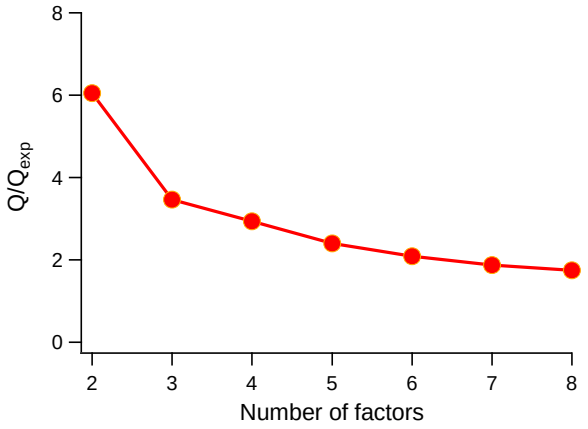

Fig. S11 Q/Q_{exp} as a function of the number of factors in OA-PMF analysis

We evaluate the environment interpretability of all the PMF runs by the following criteria. Only PMF runs that meet all the criteria below are accepted.

1. HOA should correlate with BC and NO_x (significance level of 0.05)
2. HOA should correlate better with BC and NOx than COA (significance level of 0.05)
3. Lunch peak of COA (12 p.m.) should be higher than the concentration in the morning (9 a.m.)
4. Mass spectra of COA is more similar with the reference COA than HOA (assessed by Kendall-Tau)
5. Mass spectra of HOA is more similar with the reference HOA than COA (assessed by Kendall-Tau)

Thus, we accept 451 runs and take the average profiles and time series as the final OA-PMF solution. The averaged residuals and scaled residuals of the profiles are displayed in Fig. S12 (a) and (b), respectively. The daily residual of m/z 60 and m/z 115 are displayed in Fig. S12 (c) and (d). The residual profiles exhibit no sign of significant unexplained primary fragments, suggesting the primary sources are well resolved. No significant trend of m/z 115 is observed. The daily average m/z 60 shows a slightly higher level for the first period with very large variations. This may due to the uncertainties in PMF analysis or a bit more biomass burning activities, which is similar with the trend of large particles in the Size-PMF (Regional-related 1 factor). However, considering the low m/z 60 concentrations and residuals as well as the large size of biomass burning particles, it will not significantly affect the primary source estimations in this study.

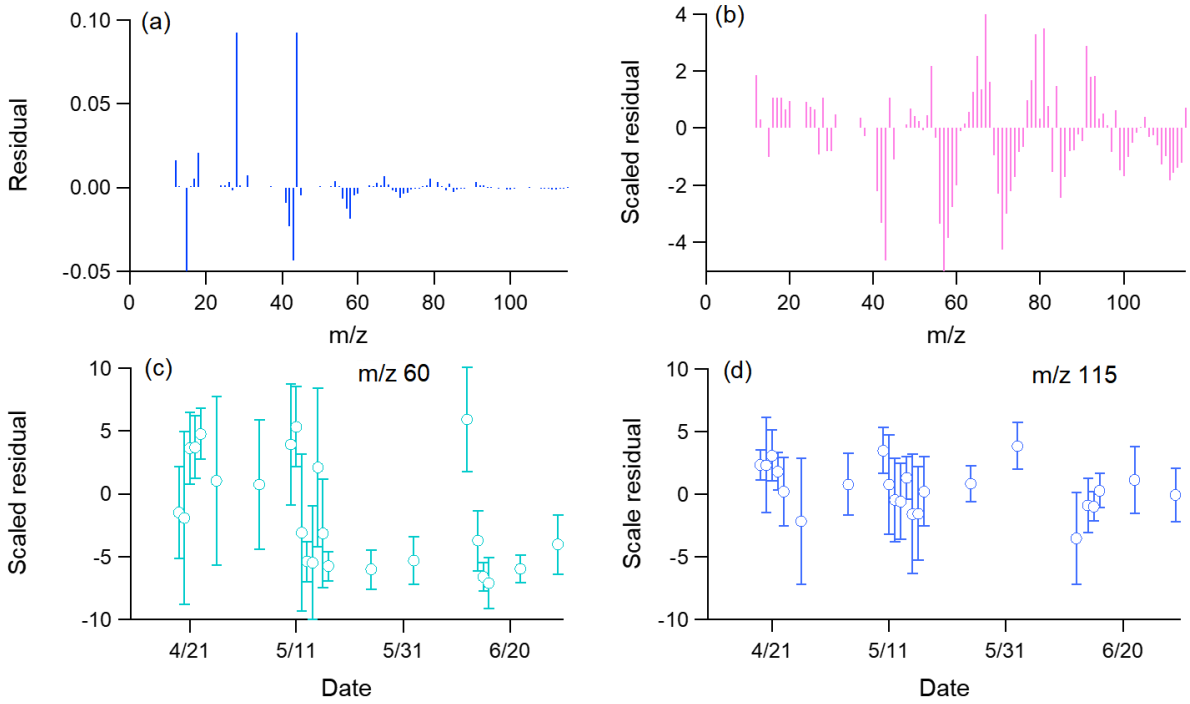

Fig. S12 Residual (a) and scaled residual (b, defined as residual to uncertainty) of OA-PMF. Daily average scaled residual of fragments of m/z 60 and 115 are displayed in (c) and (d). The round dots represent the daily average scaled residual and the error bars represent one standard variation

2.3 Other supporting information

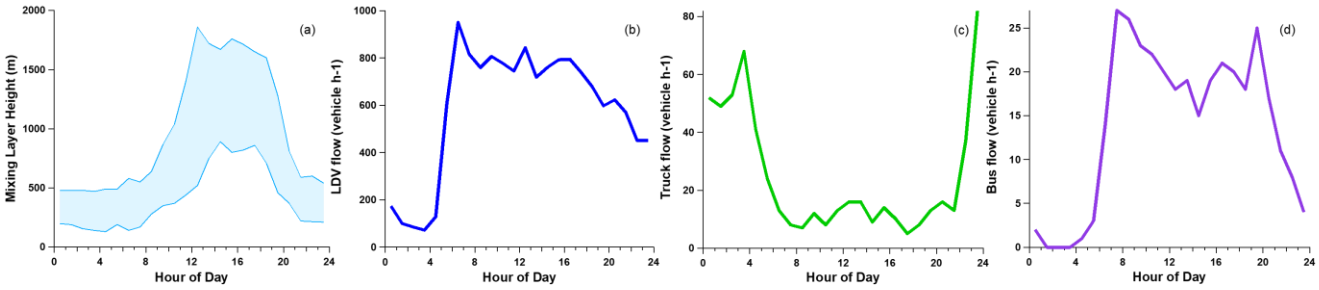

Fig. S13 Diurnal patterns of (a) mixing layer height (hourly height within 25th and 75th percentiles), (b) light-duty vehicle flow, (c) truck flow, and (d) bus flow during sampling period

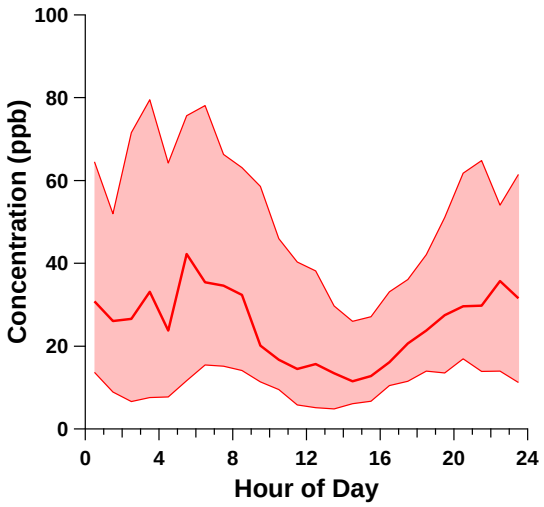

Fig. S14 Diurnal patterns of NOx (a) in winter time (Dec 1st, 2018 to Feb 28th, 2019). The range represented hourly concentrations within 25th and 75th percentiles.

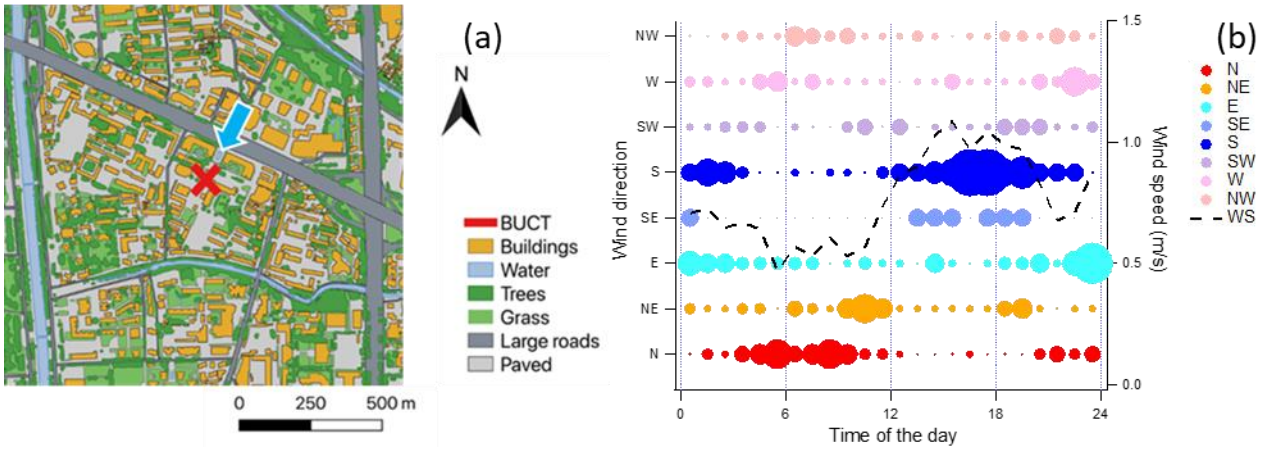

Fig. S15 (a) Sampling site and surrounding environment (modified from Kokkonen et al. (2019) with authors'permission) and, (b) wind frequencies and wind speed for different time of the day in the sampling period. The area of dots are proportional to the wind frequencies. N freq. = North (337.5° to 22.5°) wind frequencies, NE freq. = North East (22.5° to 67.5°) wind frequencies, E freq. = East (67.5° to 112.5°) wind frequencies, SE freq. = South East (112.5° to 157.5°) wind frequencies, S freq. = South (157.5° to 202.5°) wind frequencies, SW freq. = South West (202.5° to 247.5°) wind frequencies, W freq. = West (247.5° to 292.5°)wind frequencies, NW freq. = North West (292.5° to 337.5°)wind frequencies, and WS = wind speed

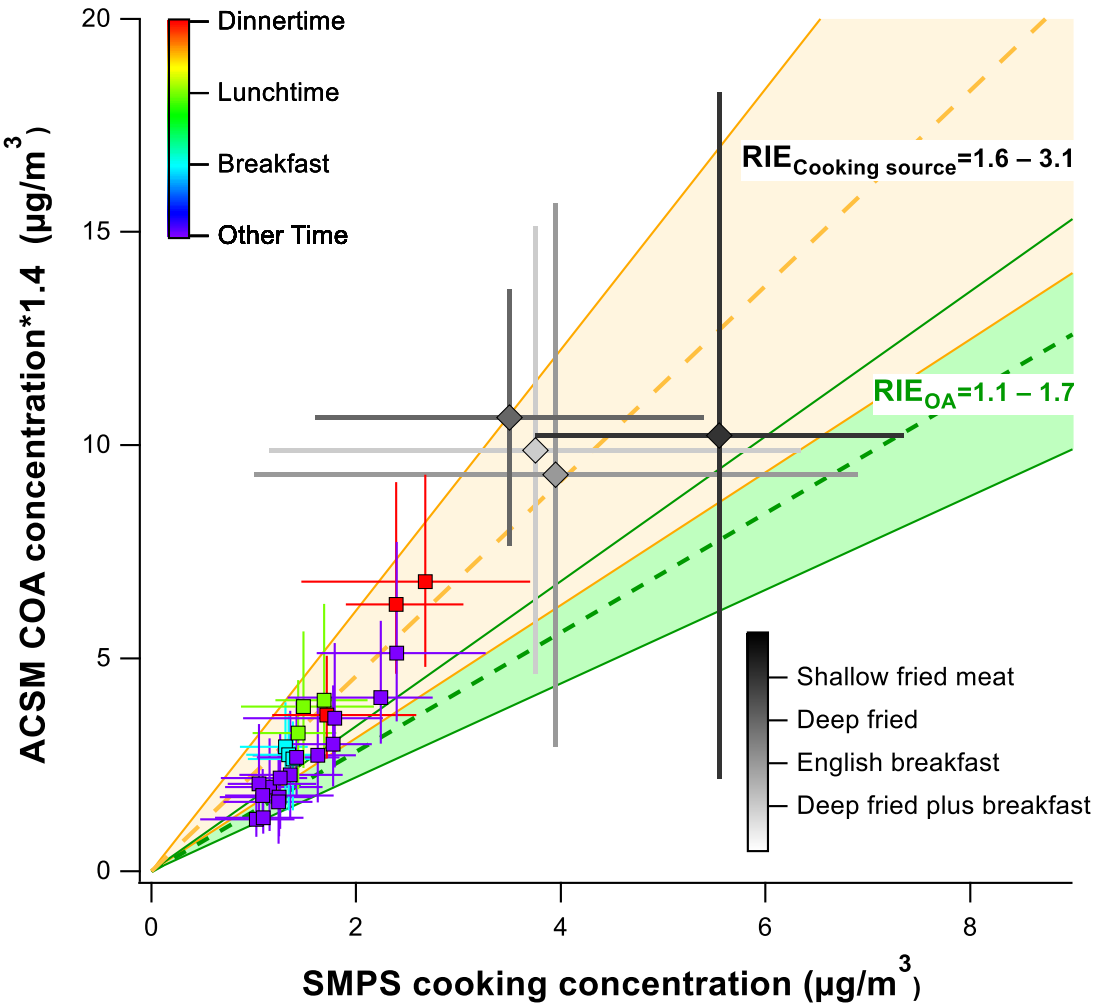

Fig. S16 The comparison of relative ionization efficiency of COA from this study and from cooking emission source tests. Square dots represented the median ACSM COA and SMPS cooking concentrations of the time of the day and coloured with different cooking hours. Error bars represent 25th and 75th percentiles. The diamonds represented the AMS and SMPS concentrations from cooking emission source tests (shown in black) and the error bars means the standard deviations of different experiments (Reyes-Villegas et al., 2018). In this plot, the concentrations and error bars from cooking source tests are multiplied with a factor of 0.5. The green and orange regions showed the RIEs for OA typically applied (Xu et al., 2018) and cooking source test (Reyes-Villegas et al., 2018). The yellow and green dash line represent the average RIE_{COA} of 2.29 from cooking sources tests and typical default RIE_{OA} of 1.4.

3. Gas phase molecular marker

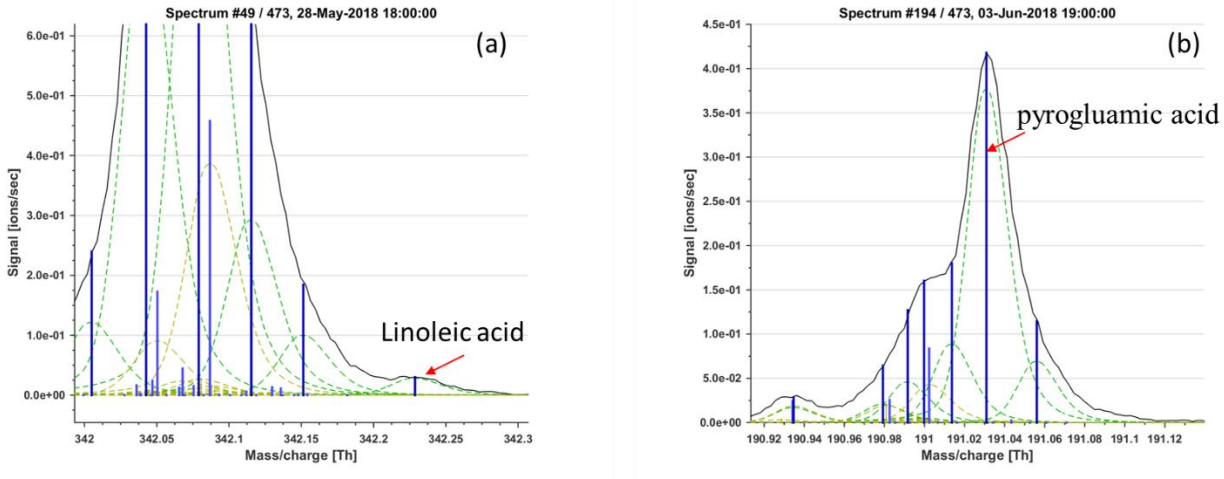

Fig. S17 Peak fitting of (a) linoleic acid ($C_{18}H_{32}O_2$) and (b) pyrogluamic acid ($C_5H_7NO_3$)

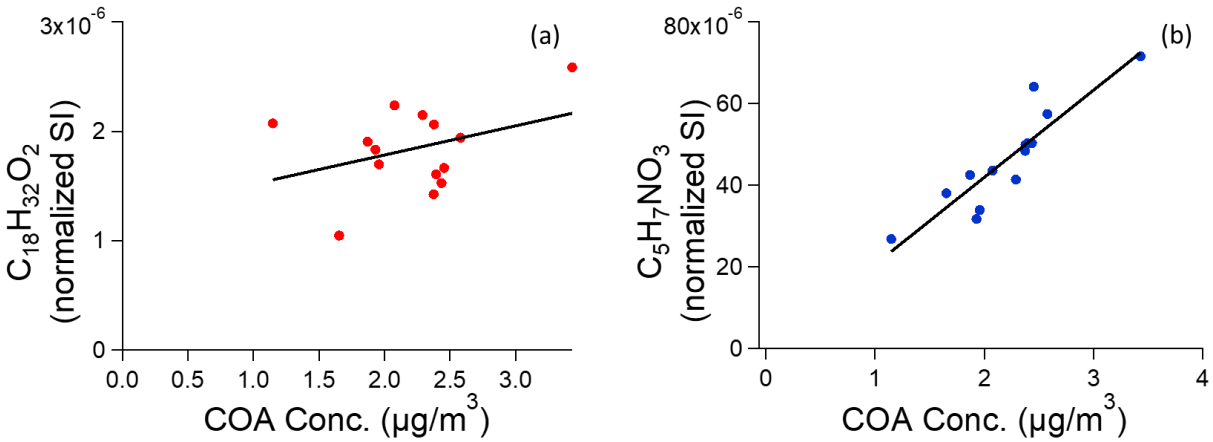

Fig. S18 Daily comparison between COA mass concentration and normalized signal intensity of (a) linoleic acid ($C_{18}H_{32}O_2$) and (b) pyrogluamic acid ($C_5H_7NO_3$). The normalized signals intensities are defined as the ratio of the raw signal intensities of those compounds to the total reagent ions (sum of NO_3^-, $HNO_3 \cdot NO_3^-$ and $(HNO_3)_2 \cdot NO_3^-$). Daily averaged concentrations are applied due to it is less affected by diurnal variations of temperature and photochemistry. To compare with gas phase procurers in a long period, here COA concentration was extracted from all sampling days, which has a good correlation with the COA extracted from non-NPF days in this study (Slope=0.99, r=0.89).

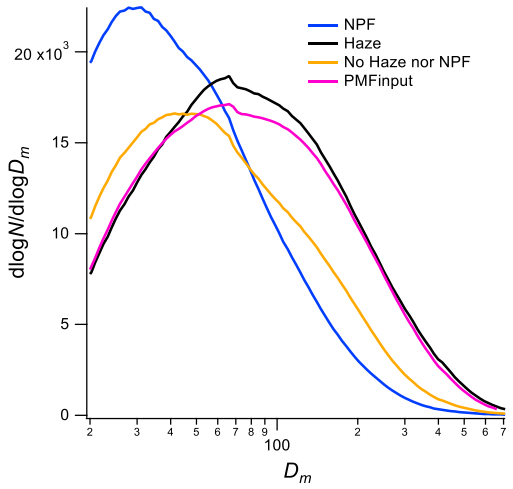

Fig. S19 Average particle size distribution of NPF days, Haze days, no Haze nor NPF event days and days used in PMF.

Reference

Canagaratna, M. R., Jayne, J. T., Ghertner, D. A., Herndon, S., Shi, Q., Jimenez, J. L., Silva, P. J., Williams, P., Lanni, T., Drewnick, F., Demerjian, K. L., Kolb, C. E., and Worsnop, D. R.: Chase Studies of Particulate Emissions from in-use New York City Vehicles, Aerosol Science and Technology, 38, 555-573, 10.1080/02786820490465504, 2004.

Crippa, M., Canonaco, F., Slowik, J. G., El Haddad, I., DeCarlo, P. F., Mohr, C., Heringa, M. F., Chirico, R., Marchand, N., Temime-Roussel, B., Abidi, E., Poulain, L., Wiedensohler, A., Baltensperger, U., and Prévôt, A. S. H.: Primary and secondary organic aerosol origin by combined gas-particle phase source apportionment, Atmospheric Chemistry and Physics, 13, 8411-8426, 10.5194/acp-13-8411-2013, 2013a.

Crippa, M., DeCarlo, P. F., Slowik, J. G., Mohr, C., Heringa, M. F., Chirico, R., Poulain, L., Freutel, F., Sciare, J., Cozic, J., Di Marco, C. F., Elsasser, M., Nicolas, J. B., Marchand, N., Abidi, E., Wiedensohler, A., Drewnick, F., Schneider, J., Borrmann, S., Nemitz, E., Zimmermann, R., Jaffrezo, J. L., Prévôt, A. S. H., and Baltensperger, U.: Wintertime aerosol chemical composition and source apportionment of the organic fraction in the metropolitan area of Paris, Atmospheric Chemistry and Physics, 13, 961-981, 10.5194/acp-13-961-2013, 2013b.

Hu, W., Hu, M., Hu, W. W., Zheng, J., Chen, C., Wu, Y. S., and Guo, S.: Seasonal variations in high time-resolved chemical compositions, sources, and evolution of atmospheric submicron aerosols in the megacity Beijing, Atmospheric Chemistry and Physics, 17, 9979-10000, 10.5194/acp-17-9979-2017, 2017.

Kokkonen, T. V., Kurppa, M., Kerminen, V.-M., Wang, Y., Lin, Z., Chao, Y., and Kulmala, M.: Seasonal variation of the radiative effect of haze on the urban boundary layer height and heat island in Beijing, Atmos. Chem. Phys. Discuss., 2019.

Mohr, C., Huffman, J. A., Cubison, M. J., Aiken, A. C., Docherty, K. S., Kimmel, J. R., Ulbrich, I. M., Hannigan, M., and Jimenez, J. L.: Characterization of Primary Organic Aerosol Emissions from Meat Cooking, Trash Burning, and Motor Vehicles with High-Resolution Aerosol Mass Spectrometry and Comparison with Ambient and Chamber Observations, Environmental Science & Technology, 43, 2443-2449, 10.1021/es8011518, 2009.

Pieber, S. M., El Haddad, I., Slowik, J. G., Canagaratna, M. R., Jayne, J. T., Platt, S. M., Bozzetti, C., Daellenbach, K. R., Frohlich, R., Vlachou, A., Klein, F., Dommen, J., Miljevic, B., Jimenez, J. L., Worsnop, D. R., Baltensperger, U., and Prevot, A. S.: Inorganic Salt Interference on CO2(+) in Aerodyne AMS and ACSM Organic Aerosol Composition Studies, Environ Sci Technol, 50, 10494-10503, 10.1021/acs.est.6b01035, 2016.

Reyes-Villegas, E., Bannan, T., Le Breton, M., Mehra, A., Priestley, M., Percival, C., Coe, H., and Allan, J. D.: Online Chemical Characterization of Food-Cooking Organic Aerosols: Implications for Source Apportionment, Environ Sci Technol, 52, 5308-5318, 10.1021/acs.est.7b06278, 2018.

Sage, A. M., Weitkamp, E. A., Robinson, A. L., and Donahue, N. M.: Evolving mass spectra of the oxidized component of organic aerosol: results from aerosol mass spectrometer analyses of aged diesel emissions, Atmos. Chem. Phys., 8, 1139-1152, 10.5194/acp-8-1139-2008, 2008.
Sun, Y., Xu, W., Zhang, Q., Jiang, Q., Canonaco, F., Prévôt, A. S. H., Fu, P., Li, J., Jayne, J., Worsnop, D. R., and Wang, Z.: Source apportionment of organic aerosol from 2-year highly time-resolved measurements by an aerosol chemical speciation monitor in Beijing, China, Atmospheric Chemistry and Physics, 18, 8469-8489, 10.5194/acp-18-8469-2018, 2018.
Ulbrich, I. M., Canagaratna, M. R., Zhang, Q., Worsnop, D. R., and Jimenez, J. L.: Interpretation of organic components from Positive Matrix Factorization of aerosol mass spectrometric data, Atmos. Chem. Phys., 9, 2891-2918, 10.5194/acp-9-2891-2009, 2009.
Xu, W., Lambe, A., Silva, P., Hu, W. W., Onasch, T., Williams, L., Croteau, P., Zhang, X., Renbaum-Wolff, L., Fortner, E., Jimenez, J. L., Jayne, J., Worsnop, D., and Canagaratna, M.: Laboratory evaluation of species-dependent relative ionization efficiencies in the Aerodyne Aerosol Mass Spectrometer, Aerosol Science and Technology, 52, 626-641, 10.1080/02786826.2018.1439570, 2018.